Article

Discovery Medicine 2026; 38(206): 826–839
https://doi.org/10.24976/Discov.Med.202638206.68

Construction of a Lipid Metabolism-Related Gene-Based Prognostic Model for Gastric Cancer and Evaluation of Its Clinical Utility

Shengjun Huang[1], Xiaofen Chen[2], Mingzhi Hong[1], Juan Ma[1,*]

[1]Department of Gastroenterology and Hepatology, Guangdong Provincial People's Hospital (Guangdong Academy of Medical Sciences), Southern Medical University, 510080 Guangzhou, Guangdong, China
[2]Department of Gastroenterology, Medical College, Shantou University, 515063 Shantou, Guangdong, China
*Correspondence: majuan@gdph.org.cn (Juan Ma)
Submitted: 5 November 2025 Revised: 9 January 2026 Accepted: 16 January 2026 Published: 20 March 2026

Background: Gastric cancer remains a lethal malignancy, and lipid metabolic reprogramming is increasingly recognized as a key driver of its progression. However, existing lipid metabolism-related genes (LMGs) signatures lack robust external validation. In this study, we identified differentially expressed LMGs, constructed and externally validated a prognostic model, and evaluated its clinical relevance with respect to the tumor microenvironment, immune escape, and drug sensitivity, while also exploring potential therapeutic agents.

Methods: LMGs were obtained from the Gene Set Enrichment Analysis (GSEA) repository. Transcriptome data derived from The Cancer Genome Atlas (TCGA) Stomach Adenocarcinoma cohort were systematically analyzed to identify genes exhibiting significant expression differences. Functional characterization and biological pathway interpretation were subsequently performed based on the Gene Ontology and Kyoto Encyclopedia of Genes and Genomes databases. Prognosis-related genes were initially screened using univariable Cox regression analysis, after which a least absolute shrinkage and selection operator approach was employed to construct a risk prediction model. The predictive capacity of the constructed model was systematically evaluated using time-to-event analyses, discrimination assessment based on Receiver Operating Characteristic (ROC) methodology, and multivariable independence testing. Furthermore, a clinically oriented nomogram was established by integrating relevant clinicopathological parameters to improve translational utility. Differences in biological pathway activity, immune-related responses, and susceptibility to chemotherapeutic agents across stratified risk categories were systematically explored using gene set enrichment analysis, the Tumor Immune Dysfunction and Exclusion algorithm, and drug response data derived from the Genomics of Drug Sensitivity in Cancer resource.

Results: A total of 179 differential expression lipid metabolism–associated genes were detected. Subsequent functional enrichment analyses revealed that these genes are primarily involved in lipid droplet organization, fatty acid and sphingolipid metabolism, and the peroxisome proliferator-activated receptor (PPAR) signaling pathway. A prognostic model was established based on eleven key genes, and patients stratified into the high-risk subgroup exhibited markedly reduced overall survival compared with the low-risk subgroup in both the training and the GSE15459 validation dataset. The prognostic model showed the area under the ROC curve (AUC) of 0.618, 0.688, and 0.734 for 1-year, 3-year, and 5-year survival intervals, respectively, with a nomogram C-index of 0.6803. Immune characterization combined with GSEA indicated that patients classified as the high-risk subgroup exhibited significant activation of pathways associated with the extracellular matrix and focal adhesion with elevated Tumor Immune Dysfunction and Exclusion (TIDE), T-cell dysfunction, and immune-exclusion scores, whereas low-risk patients showed enrichment in amino acid metabolism and DNA repair pathways, higher microsatellite instability (MSI), and distinct drug sensitivities. Analysis of chemotherapeutic responsiveness indicated that individuals classified as the high-risk subgroup exhibited increased sensitivity to 5-fluorouracil, afatinib, and docetaxel, whereas low-risk patients showed greater sensitivity to dasatinib, AZD1332, and BMS-754807.

Conclusion: We developed and validated an 11-gene lipid metabolism–based prognostic model for gastric cancer that demonstrated strong predictive performance and clinical applicability. The signature stratifies patients based on risk, reflects immune escape features and chemotherapy sensitivity, and holds potential as a tool for personalized prognosis and therapeutic decision-making.

Keywords: gastric cancer; lipid metabolism-related genes; prognostic model; risk stratification; tumor microenvironment

Introduction

Gastric cancer (GC) is one of the most prevalent malignancies globally and represents a leading cause of cancer-associated mortality. In 2022, it ranked fifth globally in both incidence and mortality among all cancers [1]. Most patients with gastric cancer are diagnosed at an advanced stage, characterized by elevated risks of recurrence and metastasis, resulting in an approximate 5-year overall survival rate of 30% [2,3]. Although chemotherapy and radiotherapy have enhanced disease control, targeted therapies and immunotherapies have shown promising efficacy in patients with advanced stages [3,4]. However, overall treatment outcomes remain suboptimal, and long-term survival continues to pose a significant clinical challenge [5].

Prognostic models for GC have attracted growing interest as tools for patient risk stratification and clinical decision-making. Among these, the tumor–node–metastasis (TNM) scheme, established by the American Joint Committee on Cancer (AJCC), remains the most widely utilized classification framework [6]. Nevertheless, considerable heterogeneity exists in clinical outcomes among patients with similar TNM stages, underscoring the limitations of solely relying on this system. Traditional clinical indicators, including patient characteristics (e.g., age and gender), pathological parameters (e.g., lymph node involvement and tumor differentiation), and hematological indicators like carcinoembryonic antigen (CEA) and carbohydrate antigens (CA19-9, CA12-5, CA72-4), are routinely applied for prognostic evaluation; however, their predictive precision remains suboptimal.

Lipids, generally defined as small-molecule metabolites with molecular weights below 1500 Da, play an essential role in cellular energy supply, membrane biosynthesis, and signal transduction [7]. Growing evidence highlights that aberrant lipid metabolic processes constitute a defining feature of malignancies and are intimately linked to the initiation and advancement of GC [8–11]. For example, aberrant expression of genes involved in glycerophospholipid metabolism has been linked to key malignant phenotypes of GC, including metastasis, chemoresistance, and recurrence [10]. Additionally, leptin-induced phosphorylation of ANGPTL4 has been shown to enhance lipoprotein lipase (LPL)-mediated lipid uptake, thereby promoting lymph node metastasis in GC [11].

With the expanding application of bioinformatics in oncology, the integration of metabolomic and transcriptomic data has emerged as a powerful approach to characterize cancer metabolic landscapes and improve prognostic assessment [12,13]. Zhou *et al.* [14] highlighted the significance of lipid metabolic remodeling in Hepatitis B virus (HBV)-driven hepatocellular carcinoma and subsequently developed a lipid metabolism–based prognostic model to stratify patients. Similarly, studies in renal cell carcinoma have indicated that dysregulation of lipid metabolism-related genes (LMGs) contributes to disease progression, is associated with heightened immune signaling, and predicts worse clinical outcomes [15].

In the context of GC, Liu *et al.* [16] developed a signature centered on lipid droplet metabolism–related genes (LDMRGs), though its reliability was limited by incomplete internal and external validation. Although several studies have attempted to develop gene expression–based prognostic classifiers for GC [17–19], many are limited by small sample sizes or insufficient validation, thereby restricting their generalizability and clinical applicability.

Therefore, there is a compelling need for more precise and dependable prognostic models in GC. In this study, we systematically identified GC–associated lipid metabolism genes and developed an LMG-based prognostic signature to facilitate individualized risk prediction and guide personalized treatment planning.

Materials and Methods

Data Collection

Transcriptomic profiles and matched clinical data were retrieved from The Cancer Genome Atlas (TCGA, https://portal.gdc.cancer.gov/) and the Gene Expression Omnibus (GEO, https://www.ncbi.nlm.nih.gov/geo/). The TCGA-STAD cohort, comprising 407 GC samples, served as the training cohort, while 192 cases from GSE15459 were employed for independent validation. We extracted lipid metabolism–related genes from the GSEA website (gene set ID: M27451, https://www.gsea-msigdb.org/).

Differential Expression Analysis

Transcriptomic data and clinical information from TCGA-STAD were extracted. Differentially expressed LMGs were screened via the "limma" R package (v3.52.2; Ritchie ME, Walter and Eliza Hall Institute, Melbourne, Australia) under $|\log2 \text{ fold change}| > 0.5$ and FDR < 0.05. Heatmaps produced with the "pheatmap" R package (v1.0.12; Kolde R, Tartu, Estonia) were subsequently used to depict the expression patterns of these genes.

GO and KEGG Enrichment Analyses

Gene Ontology (GO) and Kyoto Encyclopedia of Genes and Genomes (KEGG) pathway enrichment analyses were conducted with the "ClusterProfiler" R package (v4.4.4; Yu G, Southern Medical University, Guangzhou, China), with a significance thresholds set at $p < 0.05$ and $q < 0.05$ (adjusted p-value). Gene annotation mapping was achieved using the "org.Hs.eg.db" package (v3.15.0; Carlson M, Fred Hutchinson Cancer Center, Seattle, USA).

Construction of the Prognostic Risk Signature

We first screened LMGs for their association with overall survival using univariate Cox regression, as performed with the "survival" R package (v3.4-0; Therneau

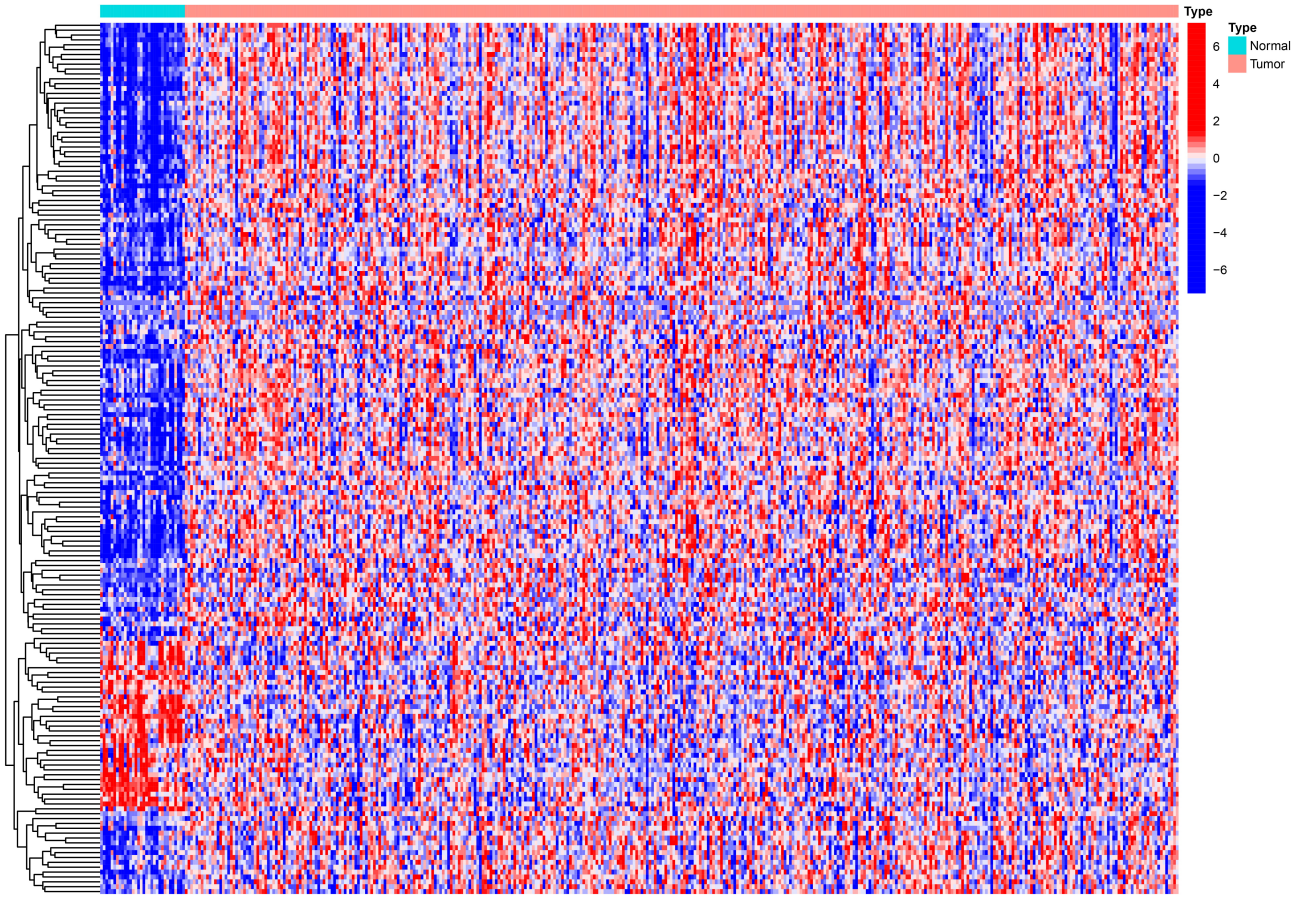

Fig. 1. Heatmap illustrating lipid metabolism–associated genes exhibiting differential expression in gastric cancer (GC).

TM, Mayo Clinic, Rochester, MN, USA). Subsequently, a prognostic signature was developed through least absolute shrinkage and selection operator (LASSO) Cox regression employing the "glmnet" (v4.1-4; Friedman J, Stanford University, Stanford, CA, USA) and "survival" packages. Using the median risk score as a cutoff, individuals in the TCGA and GEO cohorts were stratified into low- and high-risk subgroups. Kaplan–Meier survival curves for individual genes and risk strata were generated with the "survminer" R package (v0.4.9; Kassambara A, Institut de Recherche en Cancérologie, Montpellier, France). To identify factors independently associated with prognosis, univariate and multivariate Cox regression analyses were performed. The prognostic model accuracy was then quantified using time-dependent Receiver Operating Characteristic (ROC) curves and the associated the areas under the ROC curve (AUCs), implemented with the "timeROC" R package (v0.4; Blanche P, University of Lyon, Lyon, France).

Nomogram Construction

Using the "rms" R package (v6.3-0; Harrell FE, Vanderbilt University Medical Center, Nashville, TN, USA), a nomogram combining clinical features and risk scores was constructed to estimate 1-, 3-, and 5-year overall survival rates. The discriminatory ability and predictive reliability of the model were assessed via the concordance index (C-index) in combination with calibration curve analysis.

Gene Set Enrichment Analysis

Pathway-level enrichment was evaluated using GSEA implemented in R with ClusterProfiler (version 4.4.4; Southern Medical University, Guangzhou, China). The curated KEGG gene set c2.cp.kegg.v7.5.1.symbols.gmt downloaded from the GSEA molecular signatures database was analyzed.

Tumor Mutational Burden (TMB) Analysis

Somatic mutation data from the TCGA-STAD cohort were collected, and the mutational profiles distinguishing the high-risk and low-risk subgroups were visualized using the maftools package implemented in R (v2.10.0; Mayakonda A, National University of Singapore, Singapore). TMB was quantified by normalizing the overall count of somatic variants to the size of the exonic region in megabase. Individuals were subsequently classified into low-risk and high-risk subgroups using the median risk score as the cutoff.

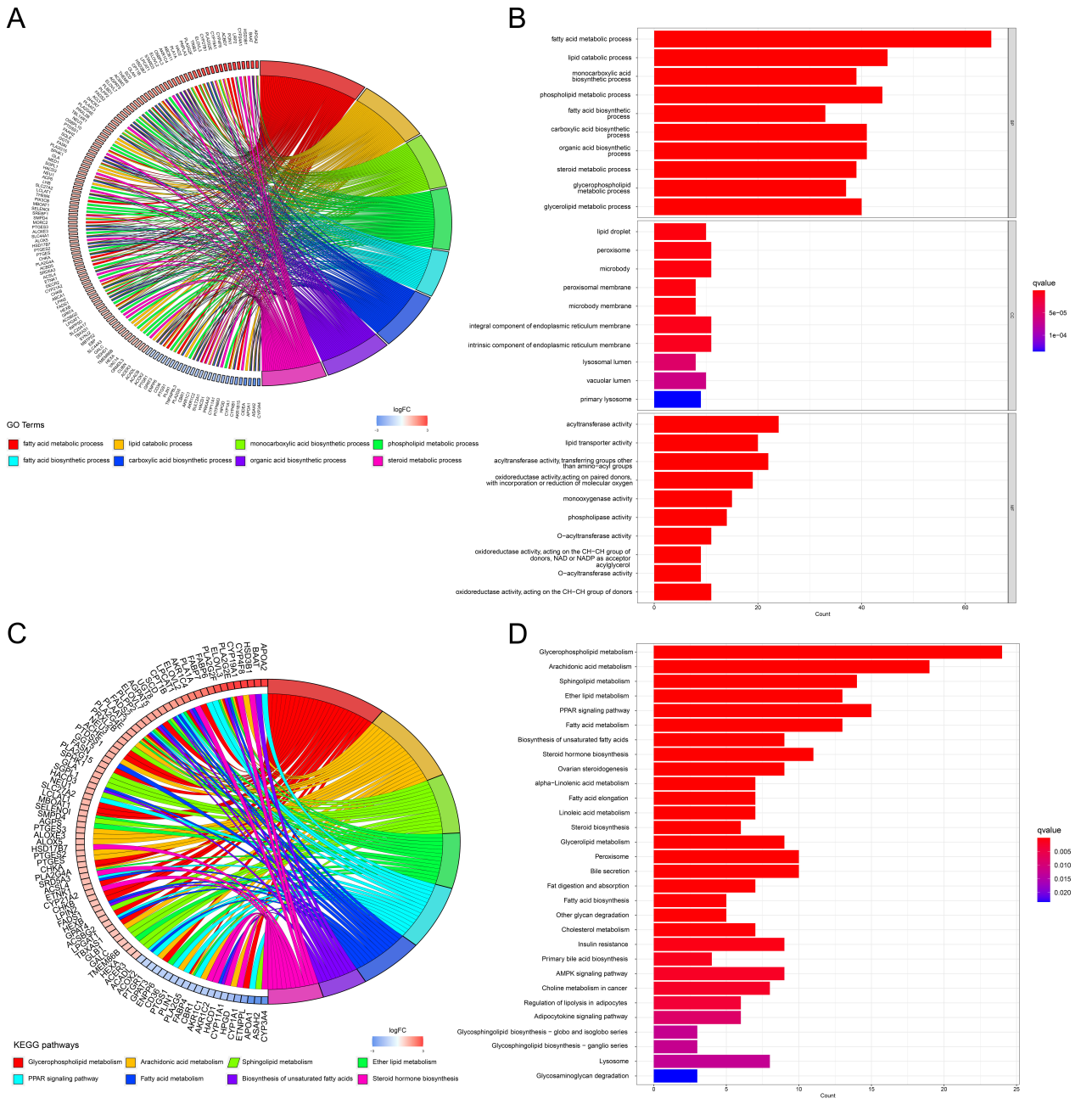

Fig. 2. Analysis of the functional roles of genes associated with lipid metabolism that exhibited differential expression. (A) Circle plot illustrating Gene Ontology (GO) enrichment of differentially expressed lipid metabolism–related genes. (B) Bar plot illustrating GO enrichment of differentially expressed lipid metabolism–related genes. (C) Circle plot illustrating Kyoto Encyclopedia of Genes and Genomes (KEGG) pathway enrichment of differentially expressed lipid metabolism–related genes. (D) Bar plot illustrating KEGG pathway enrichment of differentially expressed lipid metabolism–related genes.

Immune Cell Infiltration Analysis

The relative proportions of immune cell populations infiltrating the tumor microenvironment were estimated through application of the CIBERSORT computational framework (https://cibersort.stanford.edu/). Differential analyses between the low-risk and high-risk cohorts were subsequently conducted using the limma package in R (v3.52.2; Walter and Eliza Hall Institute, Melbourne, Australia; $p < 0.05$), and the results were graphically represented using "ggpubr" (v0.4.0; Kassambara A, Montpellier, France) and "reshape2" (v1.4.4; Wickham H, Posit PBC, Boston, MA, USA).

TIDE Immune Dysfunction and Exclusion Analysis

Indices reflecting tumor immune evasion—including T-cell dysfunction, immune exclusion, microsatellite instability, and the composite Tumor Immune Dysfunction and Exclusion (TIDE) metric—were retrieved from the

TIDE online platform (http://tide.dfci.harvard.edu/). Differences in these immunological parameters between the high-risk and low-risk subgroups were evaluated employing the Wilcoxon rank-sum test.

Drug Sensitivity Analysis

Predicted sensitivity to chemotherapeutic agents was inferred using the oncoPredict package in R (version 0.3; Maeser D, Zurich University Hospital, Switzerland), with model training based on pharmacogenomic response profiles derived from the Genomics of Drug Sensitivity in Cancer (GDSC) resource (https://www.cancerrxgene.org/). Half-maximal inhibitory concentration values were individually estimated for each patient, after which statistical differences between the low-risk and high-risk cohorts were assessed using the Wilcoxon rank-sum method.

Statistical Analysis

All statistical procedures were performed in R (v4.2.1; R Foundation for Statistical Computing, Vienna, Austria). The distribution of continuous variables was initially examined using the Shapiro–Wilk normality test. Variables following a normal distribution were compared using Student's *t* test, whereas non-normally distributed variables were compared using the Wilcoxon rank-sum test. A two-tailed *p*-value below 0.05 was considered statistically significant.

Results

Differential Expression Analysis of Lipid Metabolism-Related Genes

Transcriptomic data from TCGA were analyzed for differential expression and cross-referenced with lipid metabolism–related genes, identifying 179 lipid-associated genes with altered expression in GC. The expression profiles of these genes were visualized as a heatmap (Fig. 1), in which genes showing increased expression levels were denoted in red, whereas those exhibiting reduced expression were represented in blue.

GO and KEGG Enrichment Analyses

GO and KEGG analyses were performed to investigate the functional roles of the 179 lipid metabolism–associated genes showing differential expression. GO results revealed predominant associations with lipid droplets, peroxisomes, endoplasmic reticulum membranes, and lysosomal compartments. They were enriched in biological processes, including fatty acid metabolism, lipid catabolic processes, phospholipid metabolism, and fatty acid biosynthesis, and were functionally associated with acyltransferase activity, lipid transfer protein activity, oxidoreductase activity, monooxygenase activity, and phospholipase activity (Fig. 2A,B). KEGG signaling pathway mapping demonstrated that differentially expressed genes were predominantly concentrated in glycerophospholipid and arachidonic acid metabolism, sphingolipid metabolism, peroxisome proliferator-activated receptor (PPAR) signaling, fatty acid and unsaturated fatty acid biosynthesis, α-linolenic acid metabolism, and steroid biosynthetic pathways (Fig. 2C,D).

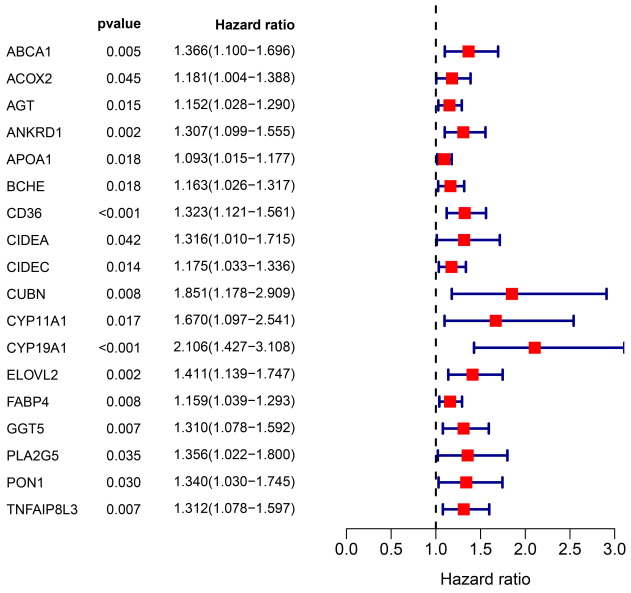

Fig. 3. Univariate Cox proportional hazards analysis of lipid metabolism–associated genes in GC. The forest plot displays genes whose expression levels were significantly correlated with overall survival (OS) within The Cancer Genome Atlas (TCGA) cohort.

Development and Evaluation of the Prognostic Risk Prediction Model

Univariate Cox proportional hazards analysis revealed 18 genes significantly correlated with overall survival (OS) in GC (Fig. 3). Subsequent LASSO Cox analysis narrowed this set down to 11 key genes (ATP Binding Cassette Subfamily A Member 1 (*ABCA1*), Ankyrin Repeat Domain 1 (*ANKRD1*), Apolipoprotein A1 (*APOA1*), Butyrylcholinesterase (*BCHE*), *CD36*, Cell Death Inducing DFFA Like Effector C (*CIDEC*), Cubilin (*CUBN*), Cytochrome P450 Family 19 Subfamily A Member 1 (*CYP19A1*), ELOVL Fatty Acid Elongase 2 (*ELOVL2*), Gamma-Glutamyltransferase 5 (*GGT5*), and Paraoxonase 1 (*PON1*)), which were integrated into a multigene prognostic signature (Fig. 4A,B). Patients were stratified into high-risk and low-risk cohorts using the median risk score as the cutoff.

Kaplan–Meier analysis demonstrated that elevated expression levels of the 11 genes were individually associated with reduced overall survival in GC patients (all $p < 0.01$) (Fig. 4C–M), supporting their role as adverse prognostic markers. To assess their combined predictive power,

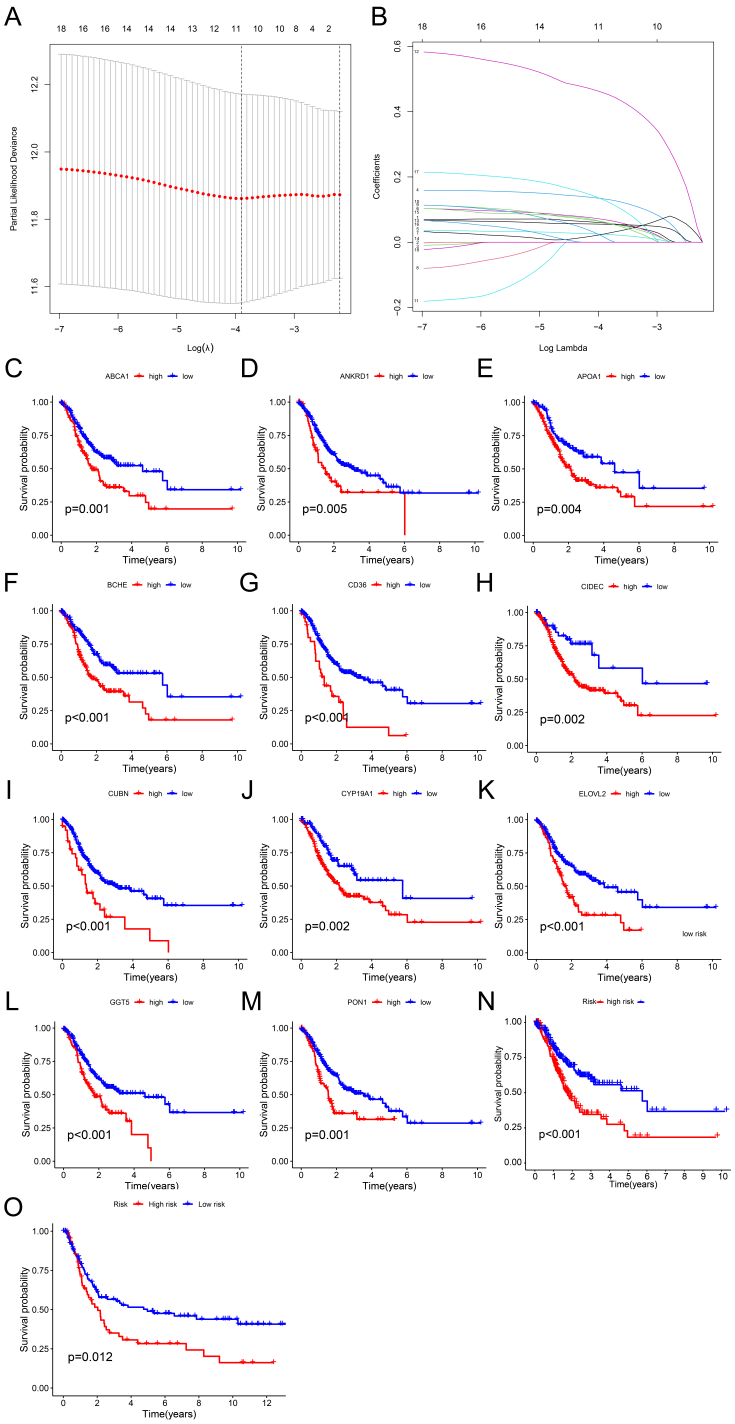

Fig. 4. Development and independent validation of a prognostic model based on lipid metabolism. (A) Coefficient trajectories of candidate genes derived from least absolute shrinkage and selection operator (LASSO) analysis. (B) Ten-fold cross-validation used to identify the optimal penalty parameter (λ) for the selection of 11 critical genes. (C) Kaplan–Meier survival curves for ATP Binding Cassette Subfamily A Member 1 (*ABCA1*). (D) Kaplan–Meier survival curves for Ankyrin Repeat Domain 1 (*ANKRD1*). (E) Kaplan–Meier survival curves for Apolipoprotein A1 (*APOA1*). (F) Kaplan–Meier survival curves for Butyrylcholinesterase (*BCHE*). (G) Kaplan–Meier survival curves for *CD36*. (H) Kaplan–Meier survival curves for Cell Death Inducing DFFA Like Effector C (*CIDEC*). (I) Kaplan–Meier survival curves for Cubilin (*CUBN*). (J) Kaplan–Meier survival curves for Cytochrome P450 Family 19 Subfamily A Member 1 (*CYP19A1*). (K) Kaplan–Meier survival curves for ELOVL Fatty Acid Elongase 2 (*ELOVL2*). (L) Kaplan–Meier survival curves for Gamma-Glutamyltransferase 5 (*GGT5*). (M) Kaplan–Meier survival curves for Paraoxonase 1 (*PON1*). (N) Kaplan–Meier curve comparing overall survival between the high- and low-risk subgroups defined by the median risk score within the TCGA cohort. (O) Validation of the prognostic model in the independent GSE15459 dataset.

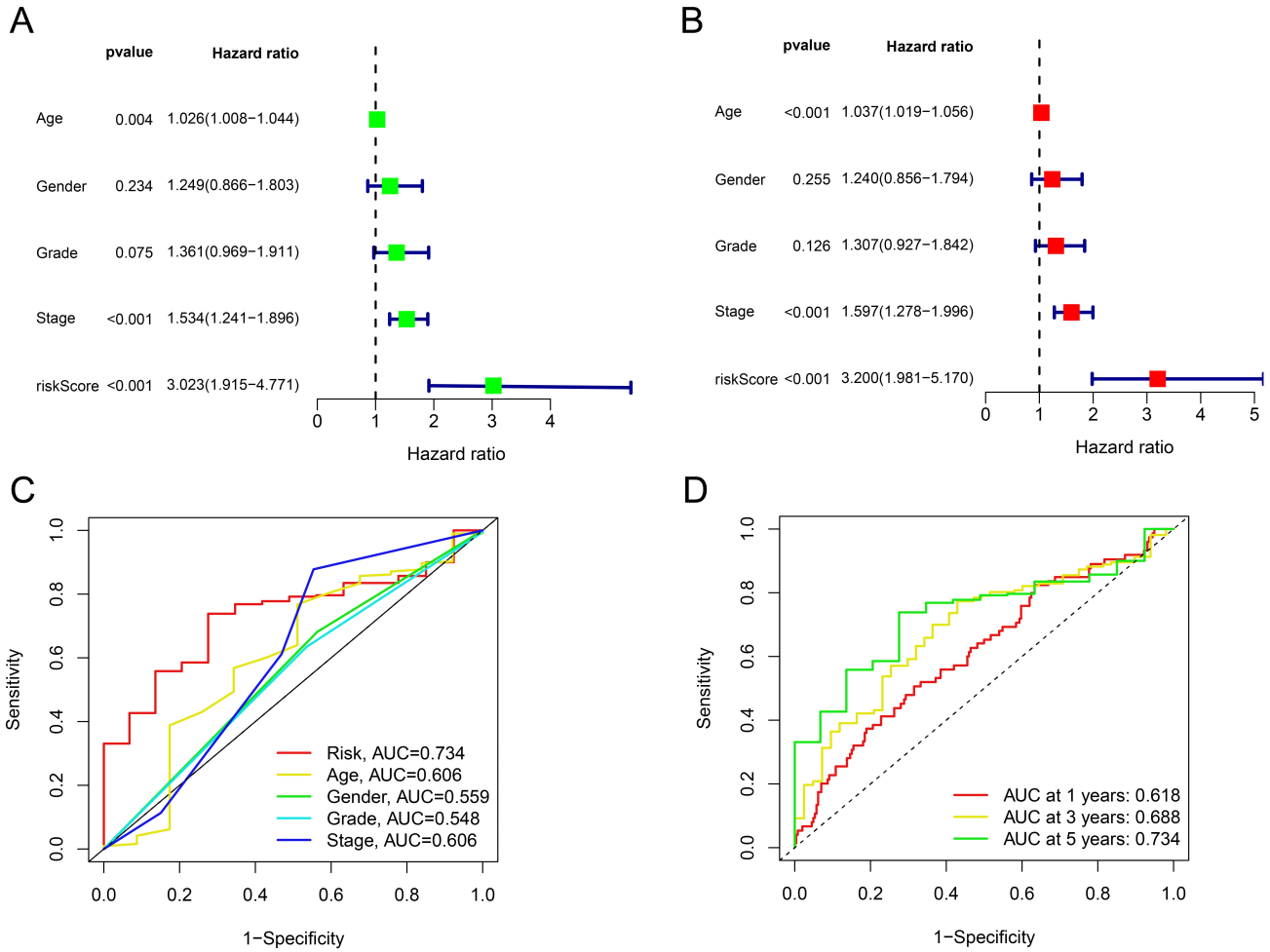

Fig. 5. Assessment of independent prognostic indicators and model predictive capability. (A) Univariate Cox regression of clinical characteristics alongside the risk score. (B) Multivariate Cox regression analysis. (C) Time-dependent Receiver Operating Characteristic (ROC) curves illustrating the comparative prognostic accuracy of clinical variables and the risk score. (D) Time-dependent ROC curves for 1-, 3-, and 5-year overall survival based on the prognostic risk model.

the 11 genes were incorporated into a multigene risk model using LASSO Cox regression. Within the TCGA cohort, patients were stratified into high- and low-risk subgroups based on the median risk score, and those in the high-risk subgroup exhibited markedly shorter overall survival ($p < 0.001$) (Fig. 4N). This risk-based classification was further validated in the independent GSE15459 cohort, in which individuals assigned to the high-risk subgroup likewise experienced significantly poorer survival outcomes ($p = 0.012$) (Fig. 4O).

Cox analyses identified that age, tumor stage, and the risk score independently predicted patient survival ($p < 0.05$) (Fig. 5A,B). The predictive accuracy of the risk model alongside clinical variables was evaluated through receiver operating characteristic ROC analysis (Fig. 5C), revealing the risk score as the most accurate predictor (AUC = 0.734), followed by age (AUC = 0.606), tumor stage (AUC = 0.606), gender (AUC = 0.559), and grade (AUC = 0.548). Time-dependent ROC analysis confirmed the model's strong prognostic performance, yielding AUC values of 0.618, 0.688, and 0.734 for predicting 1-, 3-, and 5-year overall survival, respectively (Fig. 5D).

Nomogram Construction

To improve clinical utility, a nomogram combining the 11-gene risk score with standard clinical factors (age, sex, tumor grade, and stage) was constructed (Fig. 6A). The model achieved a concordance index of 0.6803, indicating satisfactory prognostic accuracy. Calibration curves for 1-, 3-, and 5-year overall survival showed strong agreement between predicted probabilities and observed outcomes, supporting the accuracy and stability of the nomogram (Fig. 6B).

Gene Set Enrichment Analysis

GSEA was performed to probe into intrinsic biological disparities among distinct risk subgroups. Patients in the high-risk subgroup showed significant enrichment in

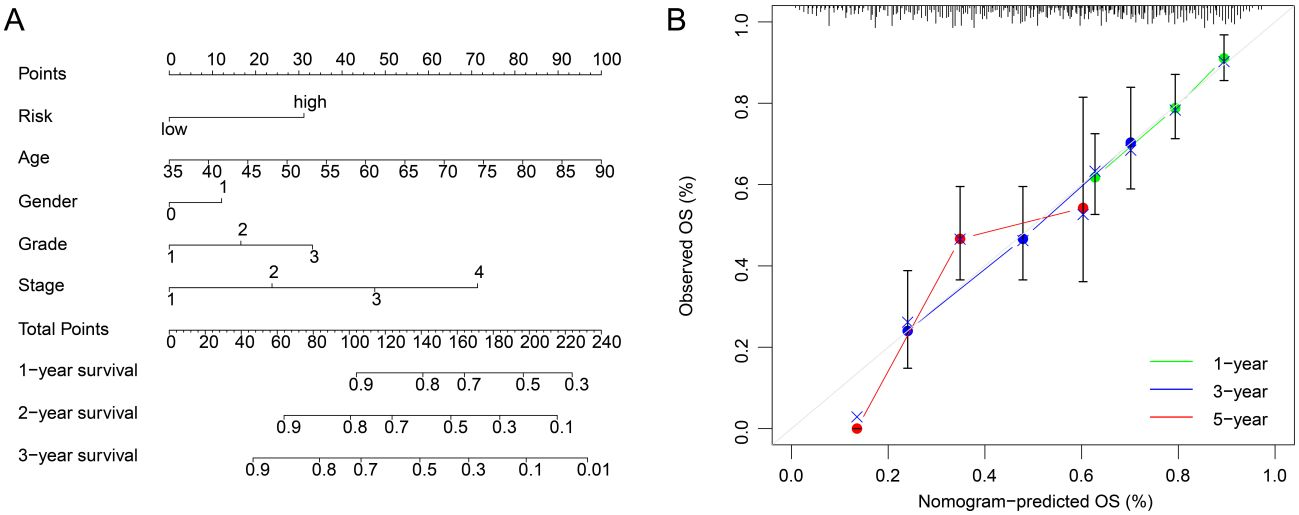

Fig. 6. Establishment and verification of a survival prediction nomogram for GC patients. (A) A nomogram incorporating an 11-gene prognostic signature and clinical parameters—encompassing age, gender, tumor differentiation grade, tumor stage, and risk score—was developed to forecast overall survival (OS) at 1, 3, and 5 years in GC patients. (B) Calibration plots were generated to evaluate the predictive performance.

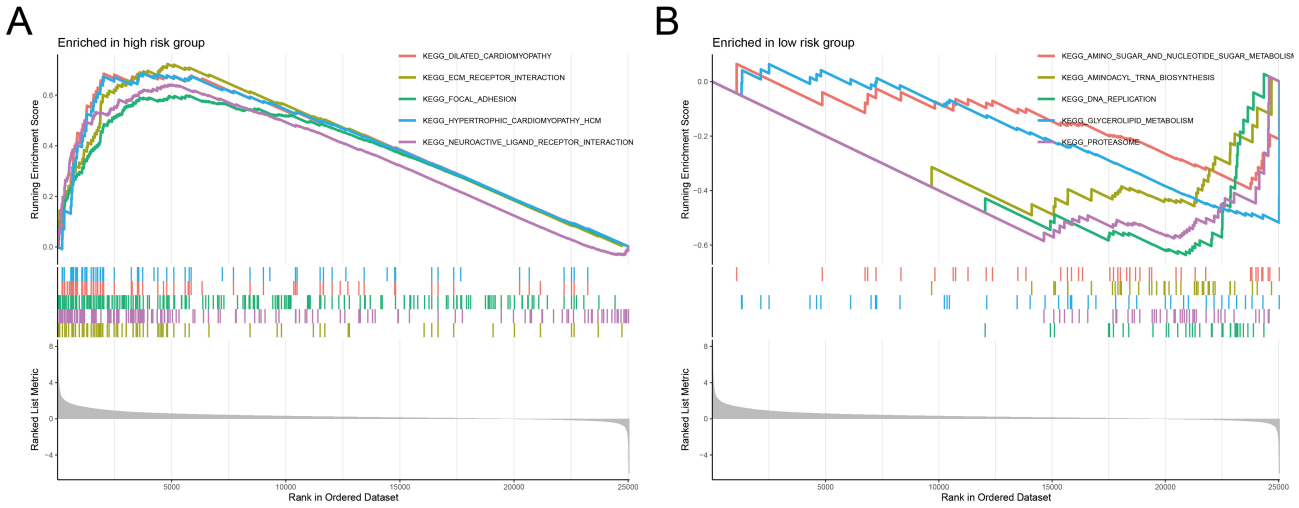

Fig. 7. Gene Set Enrichment Analysis (GSEA) of pathways enriched in the high- and low-risk subgroups. (A) Pathway enrichment signatures specific to the high-risk subgroup. (B) Pathway enrichment signatures characteristic of the low-risk subgroup.

pathways involving extracellular matrix–receptor interactions, focal adhesion, neuroactive ligand–receptor signaling, dilated cardiomyopathy, and hypertrophic cardiomyopathy (Fig. 7A), all of which are commonly linked to tumor invasiveness, cell adhesion, and aggressive disease progression. In contrast, Conversely, patients in the low-risk subgroup exhibited prominent enrichment in a panel of biological pathways, encompassing aminoacyl-tRNA biosynthesis, DNA replication, proteasome, amino sugar and nucleotide sugar metabolism, and glycerophospholipid metabolism pathways (Fig. 7B), suggesting enhanced metabolic homeostasis and biosynthetic capacity, which may contribute to better clinical outcomes.

Tumor Mutation Burden

To examine genomic variation between risk categories, somatic mutation profiles were assessed in the TCGA dataset. Among 177 high-risk patients, 158 (89.3%) harbored at least one somatic alteration (Fig. 8A), whereas 171 of 184 low-risk patients (92.9%) showed detectable mutations (Fig. 8B), indicating a slightly higher overall mutation burden in the low-risk subgroup. Across both cohorts, missense variants represented the most prevalent type of genetic alterations, followed by nonsense mutations and frameshift insertions/deletions.

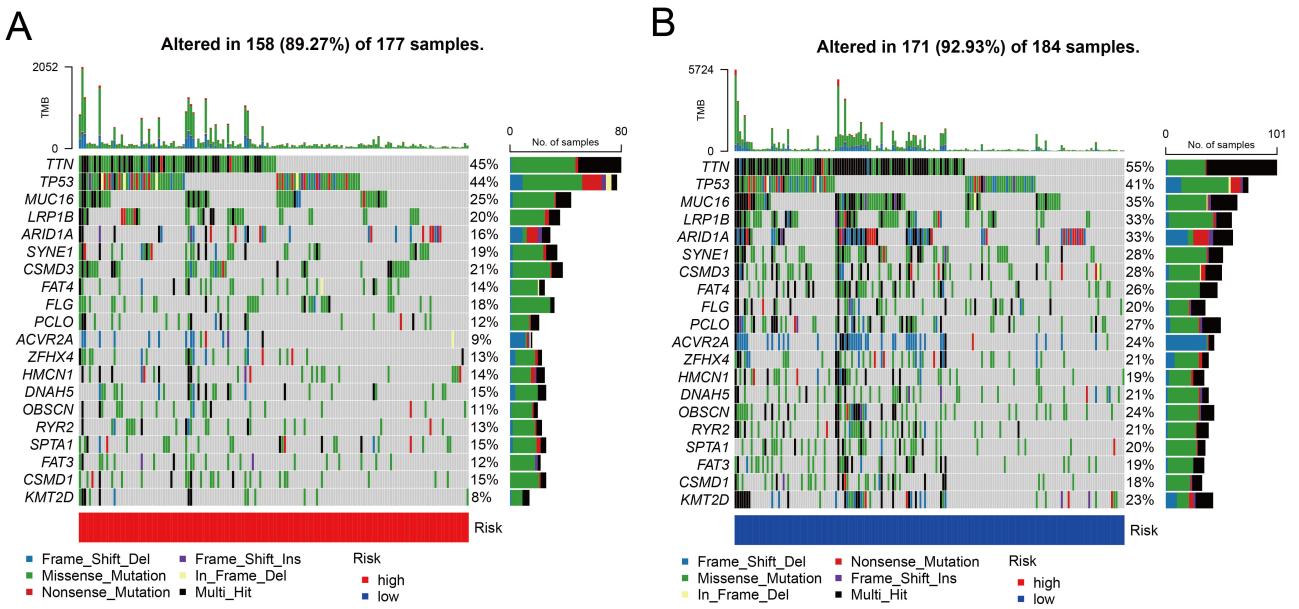

Fig. 8. Tumor mutational burden (TMB) profiling for high- and low-risk gastric cancer (GC) subgroups. (A) Somatic mutational landscape specific to the high-risk GC subgroup. (B) Somatic mutational landscape characteristic of the low-risk GC subgroup.

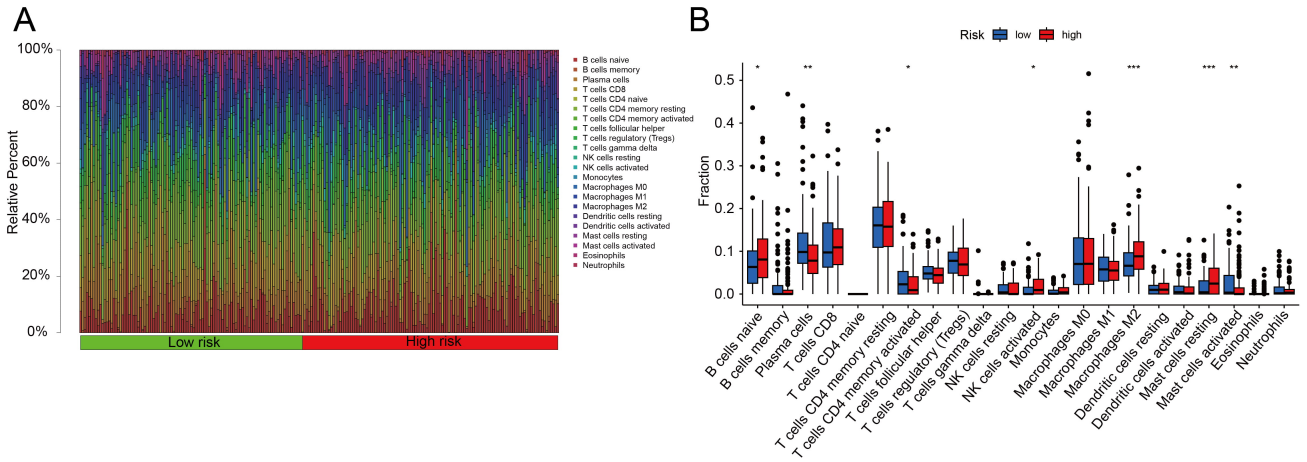

Fig. 9. Comparative immune cell composition between the high- and low-risk subgroups. (A) Bar graph depicting the predicted relative abundances of 22 immune cell subsets between the high- and low-risk subgroups, derived via the CIBERSORT computational tool. (B) Boxplots illustrating the distributional differences of the 22 immune cell subsets between the two risk subgroups. $*p < 0.05$, $**p < 0.01$, $***p < 0.001$.

Immune Cell Infiltration

In order to investigate heterogeneities within the immune microenvironment among various risk subgroups, the CIBERSORT computational tool was used to quantify 22 distinct immune cell subsets. Patients in the low-risk subgroup demonstrated markedly higher levels of infiltration by activated CD4 memory T cells and plasma cells, whereas the high-risk subgroup was characterized by prominent enrichment of resting mast cells and M2 macrophages. Heterogeneities in the composition and relative abundance of immune cells between the two subgroups are illustrated in the boxplots (Fig. 9B) and bar graph (Fig. 9A).

Immune Evasion and Immunotherapy Response

Patients in the high-risk subgroup exhibited notably increased T-lymphocyte dysfunction scores in comparison with those in the low-risk subgroup ($p < 0.01$) (Fig. 10A), which suggests more pronounced impairment of T-cell functional activity. In addition, the scores of immune exclusion were substantially elevated in the high-risk subgroup ($p < 0.001$) (Fig. 10B), suggesting strengthened barriers to the infiltration of immune cells within the tumor's immune microenvironment. Conversely, Microsatellite Instability (MSI) indices exhibited significantly elevated levels in the low-risk subgroup ($p < 0.001$) (Fig. 10C), indicating increased tumor immunogenicity. In contrast, the compos-

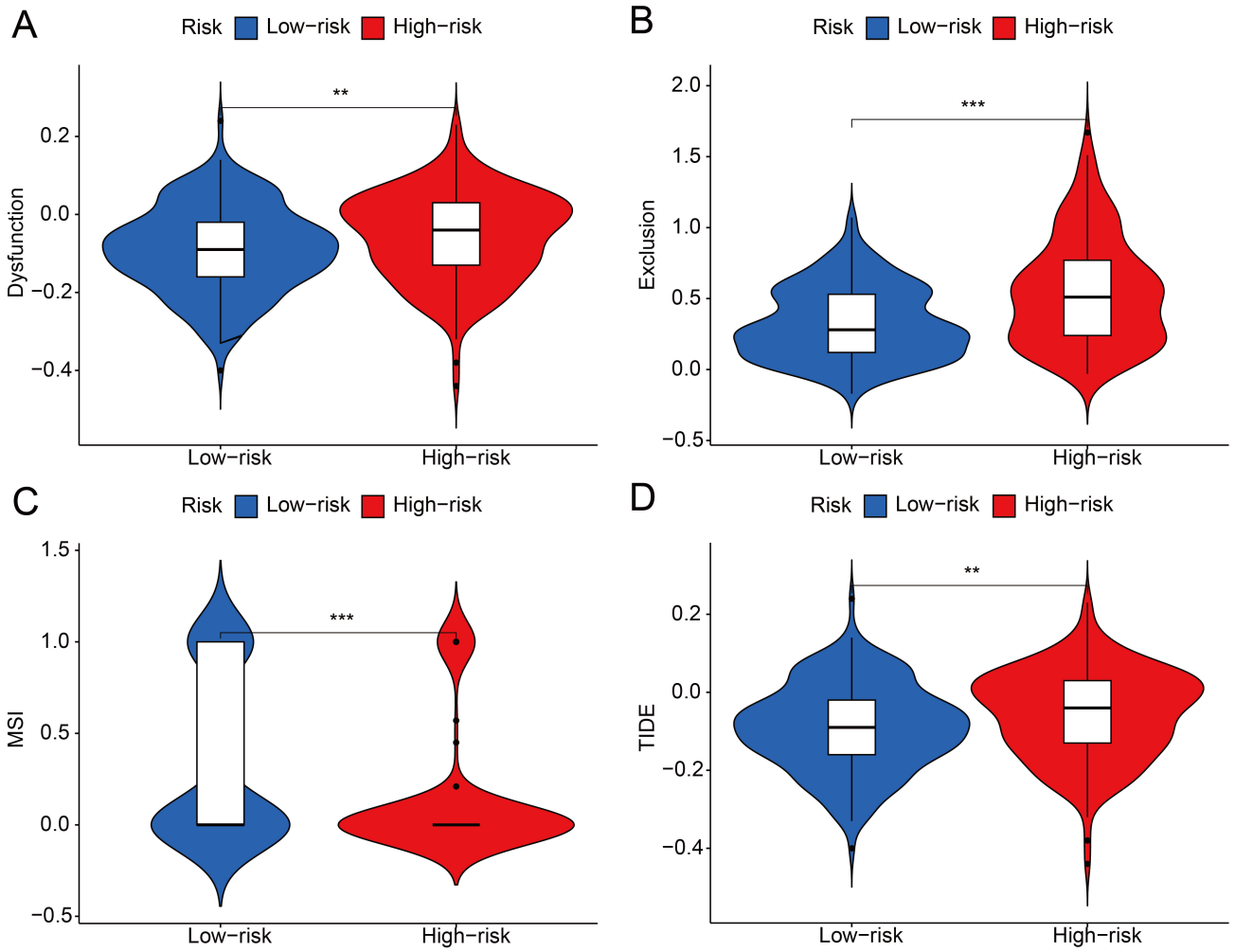

Fig. 10. Profiling of global immune escape capacity, immune dysfunction, immune exclusion, and microsatellite instability (MSI) via the Tumor Immune Dysfunction and Exclusion (TIDE) computational tool in the high- and low-risk GC subgroups. (A) T-cell dysfunction scores estimated by TIDE. (B) Immune exclusion scores estimated by TIDE. (C) MSI scores. (D) Overall TIDE scores representing tumor immune-escape potential. $^{**}p < 0.01$, $^{***}p < 0.001$.

ite TIDE index was substantially increased in the high-risk subgroup ($p < 0.01$) (Fig. 10D), reflecting a pronounced immune-evasion phenotype that could potentially compromise ICI efficacy.

Drug Sensitivity Analysis

To evaluate the prospective therapeutic implications associated with the lipid metabolism–based signature, drug sensitivity was predicted using the GDSC database. Individuals in the high-risk subgroup were anticipated to be more responsive to 5-fluorouracil, afatinib, cisplatin, cytarabine, and docetaxel (Fig. 11A–E), whereas low-risk individuals were more sensitive to dasatinib, AZD1332, and BMS-754807 (Fig. 11F–H). Collectively, these findings suggest that the risk stratification model may serve to inform the formulation of personalized therapeutic strategies for GC.

Discussion

We established an 11-gene lipid metabolism signature and validated its strong prognostic accuracy and clinical relevance in GC. The developed prognostic model exhibited robust performance in stratifying individuals into well-delineated risk subgroups characterized by substantially divergent overall survival (OS) outcomes, and retained its status as an independent prognostic factor after adjusting for well-established clinicopathological parameters. In addition, the incorporation of the signature into clinical parameters facilitated the development of a nomogram featuring robust predictive capacity, which underscores its prospective performance for tailored risk stratification and treatment decision-making.

Notably, several genes within this panel are implicated in tumor lipid reprogramming. For instance, CD36—a key transmembrane fatty acid transporter—has been documented to promote palmitate-driven tumor metastasis in GC

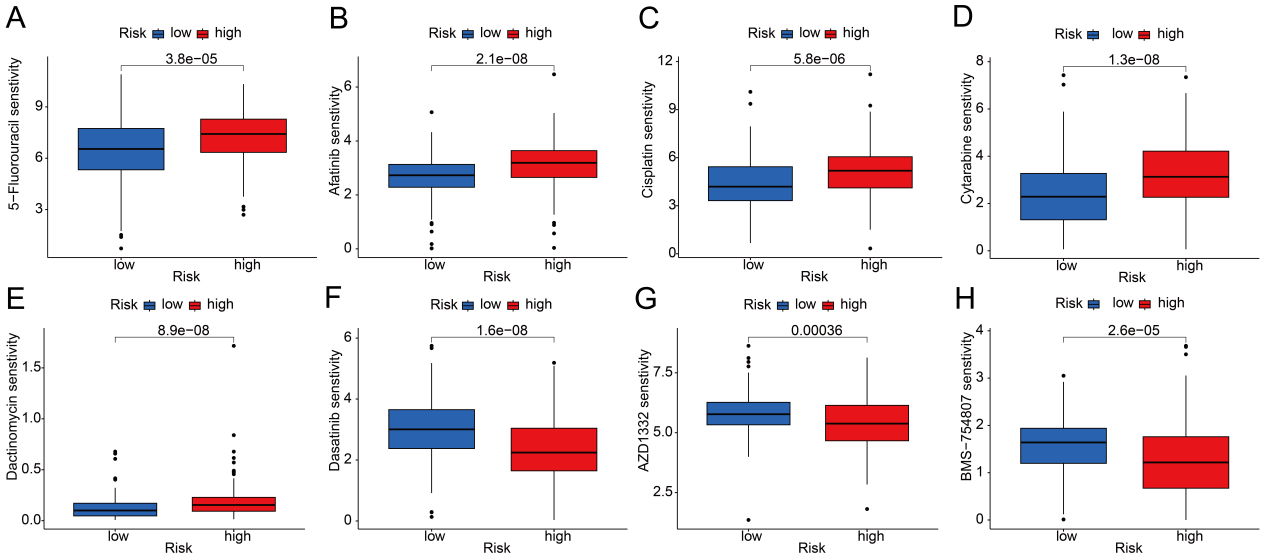

Fig. 11. Forecasted chemotherapeutic sensitivity profiles between the high- and low-risk GC subgroups, derived via the Genomics of Drug Sensitivity in Cancer (GDSC) dataset. (A) Forecasted responsiveness to 5-fluorouracil in the high-risk subgroup. (B) Predicted sensitivity to afatinib in the high-risk subgroup. (C) Predicted sensitivity to cisplatin in the high-risk subgroup. (D) Predicted sensitivity to cytarabine in the high-risk subgroup. (E) Predicted sensitivity to docetaxel in the high-risk subgroup. (F) Predicted sensitivity to dasatinib in the low-risk subgroup. (G) Predicted sensitivity to AZD1332 in the low-risk subgroup. (H) Predicted sensitivity to BMS-754807 in the low-risk subgroup.

through the AKT/GSK-3β/β-catenin signaling axis [20–22]. Similarly, APOA1 has attracted considerable attention. Xu *et al*. [23] demonstrated that APOA1 is overexpressed in GC and may drive tumor progression by remodeling cholesterol metabolism and activating the PPAR signaling pathway, a mechanism further confirmed *in vitro*. In contrast, other studies have linked downregulated APOA1 expression to aggressive GC phenotypes and poor prognosis, with serum APOA1 levels increasing following treatment [24]. These conflicting observations suggest a potentially context-dependent, spatiotemporally heterogeneous role of APOA1 in GC biology, warranting further mechanistic investigation.

ABCA1, which facilitates cholesterol export and high-density lipoprotein formation, has been implicated in colorectal cancer [25] and may similarly drive GC progression through lipid-associated mechanisms [16]. Although preliminary evidence supports its tumor-promoting role, mechanistic validation in GC remains limited. Other model genes also represent promising biological mediators; for example, *CIDEC* regulates lipid droplet metabolism and apoptosis [26,27]. *ELOVL2*, a key enzyme catalyzing the elongation of very-long-chain fatty acids, exhibits elevated expression across multiple cancer types [28,29]. *GGT5* may modulate GC development through glutathione metabolism and PI3K-Akt signaling [30]. In addition, *PON1* polymorphisms influence oxidative stress and GC risk [31], *CYP19A1* regulates estrogen biosynthesis and has been linked to GC progression [32], and *CUBN* expression correlates with GC susceptibility and may influence tumor biological behavior and clinical outcomes [33]. *BCHE* may participate in tumor-immune metabolic regulation [34], while *ANKRD1* contributes to Wnt pathway regulation and cancer metastasis [35,36]. Taken together, these genes reflect the multifaceted roles of lipid metabolism in tumor initiation, immune modulation, and metastatic dissemination.

The prognostic accuracy of our LMG-based signature was further validated in an independent GEO dataset (GSE15459), demonstrating consistent survival stratification and promising AUC metrics. Our analysis identified a marginally elevated TMB in the low-risk subgroup compared with the high-risk subgroup—an observation that appears paradoxical considering the typical association of increased TMB with genomic instability and adverse prognosis across numerous malignancies. Increasing evidence indicates that the prognostic effect of TMB is highly context-dependent and influenced by tumor-specific biology, immune-microenvironmental features, and mutation composition rather than mutation quantity alone [37]. In GC, high TMB is frequently linked to microsatellite instability–high (MSI-H) status and POLE/POLD1 mutations, both of which are known to activate robust antitumor immunity and confer favorable clinical outcomes [38]. Consistent with this observation, our findings revealed significantly elevated microsatellite instability (MSI) indices in the low-risk subgroup, which implies that the modestly increased TMB in this subgroup could reflect an immunogenic mutation profile. Prior studies have also reported that MSI-H and TMB-high gastric tumors exhibit greater

neoantigen load, stronger immune infiltration, and improved survival compared with microsatellite-stable counterparts [39].

Conversely, although the high-risk group exhibited slightly lower TMB, it may harbor more aggressive driver alterations or molecular features associated with immune evasion. Based on the TIDE computational framework, Jiang et al. validated that tumor-associated immune dysfunction and immune exclusion can substantially attenuate TMB-mediated immunogenic benefits, thereby enabling tumors with moderate or even low TMB to exhibit poor survival outcome [40]. This observation is consistent with our findings, wherein the high-risk subgroup exhibited elevated TIDE indices alongside prominent molecular signatures of immune exclusion and dysfunction. These observations imply that the reduced TMB in the high-risk subgroup likely coexists with a more immunosuppressive microenvironment, thereby reducing immune surveillance and contributing to poorer outcomes. From a clinical perspective, the co-occurrence of modestly elevated TMB and enriched MSI in the low-risk subgroup could indicate enhanced responsiveness to immune checkpoint inhibitors (ICIs). In contrast, elevated TIDE indices in the high-risk subgroup suggest a more prominent immune escape phenotype, with potentially decreased sensitivity to ICI-based immunotherapy. Collectively, these findings highlight the complex interplay among TMB, the immune landscape, and lipid-metabolism–related gene expression, underscoring the importance of integrating genomic and immunologic biomarkers when interpreting clinical outcomes or informing treatment strategies in GC.

Given that cytotoxic chemotherapy remains the cornerstone of advanced GC management [41], we further evaluated drug response patterns via GDSC-based prediction. High-risk patients were more sensitive to 5-fluorouracil, afatinib, cisplatin, cytarabine, and docetaxel, whereas low-risk patients exhibited higher sensitivity to dasatinib, AZD1332, and BMS-754807 [42,43]. These data support a model's role in informing individualized therapeutic strategies and identifying candidate agents for specific metabolic subtypes of GC.

Taken together, this study underscores the central role of lipid metabolic dysregulation in GC progression and therapeutic responsiveness. Several limitations should be acknowledged. First, the TCGA-STAD dataset provides only limited information on whether patients received radiotherapy or chemotherapy, and lacks details on specific drug regimens, preventing direct validation of predicted drug responses against actual treatments. Second, the risk model was constructed primarily from public datasets, and heterogeneity in sample sources as well as incomplete clinical records may affect its stability and generalizability. As a retrospective analysis, the model has not yet been validated in prospective, multi-center cohorts; therefore, evaluation in larger real-world populations is needed to determine its clinical utility. Moreover, the key genes incorporated in the model have not been systematically validated through functional experiments, and their precise biological roles in tumor progression remain unclear. Future research integrating multi-omics analyses with *in vitro* and *in vivo* functional experiments, alongside mechanistic investigations, may help refine and enhance the model while also informing potential metabolic–immune combinational therapeutic strategies.

Conclusion

In this study, we developed a prognostic model for GC based on lipid metabolism-related genes, and validated its reliability in an external cohort. This lipid metabolism-centered signature surpassed previous prognostic models in predictive performance, facilitated reliable stratification of patients into distinct risk subgroups, revealed heterogeneity in the tumor immune microenvironment, and laid a theoretical basis for predicting therapeutic responses to ICI-based immunotherapies and conventional chemotherapies. We further constructed a clinically applicable nomogram that integrates molecular signatures with clinical attributes of patients to improve the accuracy of individualized survival predictions and inform clinical therapeutic decision-making. This integrated approach paves the way for precision oncology in GC and could guide the development of future metabolism-targeted therapeutic strategies.

Availability of Data and Materials

The experimental data used to support the findings of this study are available from the corresponding author upon request.

Author Contributions

SH: Conceptualization, Data curation, Formal analysis, Writing—original draft. XC: Methodology, Visualization, Writing—review & editing. MH: Software, Validation, Data interpretation, Writing—review & editing. JM: Co-conceptualization, Supervision, Project administration, Funding acquisition, Writing—review & editing. All authors gave final approval of the version to be published. All authors have participated sufficiently in the work to take public responsibility for appropriate portions of the content and agreed to be accountable for all aspects of the work in ensuring that questions related to its accuracy or integrity.

Ethics Approval and Consent to Participate

Not applicable.

Acknowledgment

Not applicable.

Funding

Not applicable.

Conflict of Interest

The authors declare no conflict of interest.

References

[1] Bray F, Laversanne M, Sung H, Ferlay J, Siegel RL, Soerjomataram I, *et al*. Global cancer statistics 2022: GLOBOCAN estimates of incidence and mortality worldwide for 36 cancers in 185 countries. CA: A Cancer Journal for Clinicians. 2024; 74: 229–263. https://doi.org/10.3322/caac.21834.

[2] Smyth EC, Nilsson M, Grabsch HI, van Grieken NC, Lordick F. Gastric cancer. Lancet. 2020; 396: 635–648. https://doi.org/10.1016/S0140-6736(20)31288-5.

[3] Li H, Shen M, Wang S. Current therapies and progress in the treatment of advanced gastric cancer. Frontiers in Oncology. 2024; 14: 1327055. https://doi.org/10.3389/fonc.2024.1327055.

[4] Luo D, Liu Y, Lu Z, Huang L. Targeted therapy and immunotherapy for gastric cancer: rational strategies, novel advancements, challenges, and future perspectives. Molecular Medicine. 2025; 31: 52. https://doi.org/10.1186/s10020-025-01075-y.

[5] Burz C, Pop V, Silaghi C, Lupan I, Samasca G. Prognosis and Treatment of Gastric Cancer: A 2024 Update. Cancers. 2024; 16: 1708. https://doi.org/10.3390/cancers16091708.

[6] Liu JY, Peng CW, Yang XJ, Huang CQ, Li Y. The prognosis role of AJCC/UICC 8th edition staging system in gastric cancer, a retrospective analysis. American Journal of Translational Research. 2018; 10: 292–303.

[7] Smirnov D, Mazin P, Osetrova M, Stekolshchikova E, Khrameeva E. The Hitchhiker's Guide to Untargeted Lipidomics Analysis: Practical Guidelines. Metabolites. 2021; 11: 713. https://doi.org/10.3390/metabo11110713.

[8] Jiang Z, Gu Z, Lu X, Wen W. The role of dysregulated metabolism and associated genes in gastric cancer initiation and development. Translational Cancer Research. 2024; 13: 3854–3868. https://doi.org/10.21037/tcr-23-2244.

[9] Gupta A, Das D, Taneja R. Targeting Dysregulated Lipid Metabolism in Cancer with Pharmacological Inhibitors. Cancers. 2024; 16: 1313. https://doi.org/10.3390/cancers16071313.

[10] Chen M, Zhang C, Li H, Zheng S, Li Y, Yuan M, *et al*. PLA2G4A and ACHE modulate lipid profiles via glycerophospholipid metabolism in platinum-resistant gastric cancer. Journal of Translational Medicine. 2024; 22: 249. https://doi.org/10.1186/s12967-024-05055-4.

[11] Xiao J, Cao S, Wang J, Li P, Cheng Q, Zhou X, *et al*. Leptin-mediated suppression of lipoprotein lipase cleavage enhances lipid uptake and facilitates lymph node metastasis in gastric cancer. Cancer Communications. 2024; 44: 855–878. https://doi.org/10.1002/cac2.12583.

[12] Chen Y, Yuan H, Yu Q, Pang J, Sheng M, Tang W. Bioinformatics Analysis and Structure of Gastric Cancer Prognosis Model Based on Lipid Metabolism and Immune Microenvironment. Genes. 2022; 13: 1581. https://doi.org/10.3390/genes13091581.

[13] Li Y, Zhao J, Chen R, Chen S, Xu Y, Cai W. Integration of clinical and transcriptomics reveals programming of the lipid metabolism in gastric cancer. BMC Cancer. 2022; 22: 955. https://doi.org/10.1186/s12885-022-10017-4.

[14] Zhou L, Xia S, Liu Y, Ji Q, Li L, Gao X, *et al*. A lipid metabolism-based prognostic risk model for HBV-related hepatocellular carcinoma. Lipids in Health and Disease. 2023; 22: 46. https://doi.org/10.1186/s12944-023-01780-9.

[15] Li K, Zhu Y, Cheng J, Li A, Liu Y, Yang X, *et al*. A novel lipid metabolism gene signature for clear cell renal cell carcinoma using integrated bioinformatics analysis. Frontiers in Cell and Developmental Biology. 2023; 11: 1078759. https://doi.org/10.3389/fcell.2023.1078759.

[16] Liu M, Fang X, Wang H, Ji R, Guo Q, Chen Z, *et al*. Characterization of lipid droplet metabolism patterns identified prognosis and tumor microenvironment infiltration in gastric cancer. Frontiers in Oncology. 2023; 12: 1038932. https://doi.org/10.3389/fonc.2022.1038932.

[17] Jiang M, Fang C, Ma Y. Prognosis Risk Model Based on Pyroptosis-Related lncRNAs for Gastric Cancer. Biomolecules. 2023; 13: 469. https://doi.org/10.3390/biom13030469.

[18] Li GX, Chen YP, Hu YY, Zhao WJ, Lu YY, Wan FJ, *et al*. Machine learning for identifying tumor stemness genes and developing prognostic model in gastric cancer. Aging. 2024; 16: 6455–6477. https://doi.org/10.18632/aging.205715.

[19] Hu C, Song J, Kwok T, Nguyen EV, Shen X, Daly RJ. Proteome-based molecular subtyping and therapeutic target prediction in gastric cancer. Molecular Oncology. 2024; 18: 1437–1459. https://doi.org/10.1002/1878-0261.13654.

[20] Pan J, Fan Z, Wang Z, Dai Q, Xiang Z, Yuan F, *et al*. CD36 mediates palmitate acid-induced metastasis of gastric cancer via AKT/GSK-3β/β-catenin pathway. Journal of Experimental & Clinical Cancer Research. 2019; 38: 52. https://doi.org/10.1186/s13046-019-1049-7.

[21] Cui MY, Yi X, Zhu DX, Wu J. The Role of Lipid Metabolism in Gastric Cancer. Frontiers in Oncology. 2022; 12: 916661. https://doi.org/10.3389/fonc.2022.916661.

[22] Wang J, Li Y. CD36 tango in cancer: signaling pathways and functions. Theranostics. 2019; 9: 4893–4908. https://doi.org/10.7150/thno.36037.

[23] Xu P, Zhang Q, Zhai J, Chen P, Deng X, Miao L, *et al*. APOA1 promotes tumor proliferation and migration and may be a potential pan-cancer biomarker and immunotherapy target. Translational Oncology. 2025; 55: 102344. https://doi.org/10.1016/j.tranon.2025.102344.

[24] Li F, Han M, Gao X, Du X, Jiang C. *APOA1* mRNA and serum APOA1 protein as diagnostic and prognostic biomarkers in gastric cancer. Translational Cancer Research. 2024; 13: 2141–2154. https://doi.org/10.21037/tcr-23-1966.

[25] Fernández LP, Ramos-Ruiz R, Herranz J, Martín-Hernández R, Vargas T, Mendiola M, *et al*. The transcriptional and mutational landscapes of lipid metabolism-related genes in colon cancer. Oncotarget. 2017; 9: 5919–5930. https://doi.org/10.18632/oncotarget.23592.

[26] Lu X, Chen Y, Xie Q, Tong N. Comparative effect of high intensity interval training and moderate intensity continuous training on metabolic improvements and regulation of Cidea and Cidec in obese C57BL/6 mice. PLoS ONE. 2025; 20: e0322634. https://doi.org/10.1371/journal.pone.0322634.

[27] Liu K, Zhou S, Kim JY, Tillison K, Majors D, Rearick D, *et al*. Functional analysis of FSP27 protein regions for lipid droplet localization, caspase-dependent apoptosis, and dimerization with CIDEA. American Journal of Physiology. Endocrinology and Metabolism. 2009; 297: E1395–E1413. https://doi.org/10.1152/ajpendo.00188.2009.

[28] Tanaka K, Kandori S, Sakka S, Nitta S, Tanuma K, Shiga M, *et al*. ELOVL2 promotes cancer progression by inhibiting cell apoptosis in renal cell carcinoma. Oncology Reports. 2022; 47: 23. https://doi.org/10.3892/or.2021.8234.

[29] Dai W, Liu H, Xu X, Ge J, Luo S, Zhu D, *et al*. Genetic variants in ELOVL2 and HSD17B12 predict melanoma-specific survival. International Journal of Cancer. 2019; 145: 2619–2628. https:

//doi.org/10.1002/ijc.32194.

[30] Wang Y, Fang Y, Zhao F, Gu J, Lv X, Xu R, *et al*. Identification of *GGT5* as a Novel Prognostic Biomarker for Gastric Cancer and its Correlation With Immune Cell Infiltration. Frontiers in Genetics. 2022; 13: 810292. https://doi.org/10.3389/fgene.2022.810292.

[31] Najafi E, Pourfarzi F, Mazani M, Yazdanbod A, Rezagholizadeh K, Fazaeli A. Paraoxonase 1 polymorphisms and their relationship with gastric cancer risk: a biochemical perspective on oxidative stress. Molecular Biology Reports. 2025; 52: 472. https://doi.org/10.1007/s11033-025-10563-7.

[32] Zhou X, Meng F, Xiao L, Shen H. CYP19A1 promotes gastric cancer as part of a lipid metabolism-related gene signature related to the response of immunotherapy and prognosis. BMC Medical Genomics. 2023; 16: 228. https://doi.org/10.1186/s12920-023-01664-y.

[33] Zhao L, Wei Y, Song A, Li Y. Association study between genome-wide significant variants of vitamin B12 metabolism and gastric cancer in a han Chinese population. IUBMB Life. 2016; 68: 303–310. https://doi.org/10.1002/iub.1485.

[34] Wang S, Huang X, Zhao S, Lv J, Li Y, Wang S, *et al*. Progressions of the correlation between lipid metabolism and immune infiltration characteristics in gastric cancer and identification of BCHE as a potential biomarker. Frontiers in Immunology. 2024; 15: 1327565. https://doi.org/10.3389/fimmu.2024.1327565.

[35] Xu X, Zhong D, Wang X, Luo F, Zheng X, Feng T, *et al*. Pan-cancer integrated analysis of ANKRD1 expression, prognostic value, and potential implications in cancer. Scientific Reports. 2024; 14: 5268. https://doi.org/10.1038/s41598-024-56105-2.

[36] Diskul-Na-Ayudthaya P, Bae SJ, Bae YU, Van NT, Kim W, Ryu S. ANKRD1 Promotes Breast Cancer Metastasis by Activating NF-κB-MAGE-A6 Pathway. Cancers. 2024; 16: 3306. https://doi.org/10.3390/cancers16193306.

[37] Valero C, Lee M, Hoen D, Wang J, Nadeem Z, Patel N, *et al*. The association between tumor mutational burden and prognosis is dependent on treatment context. Nature Genetics. 2021; 53: 11–15. https://doi.org/10.1038/s41588-020-00752-4.

[38] Zhu M, Cui H, Zhang L, Zhao K, Jia X, Jin H. Assessment of *POLE* and *POLD1* mutations as prognosis and immunotherapy biomarkers for stomach adenocarcinoma. Translational Cancer Research. 2022; 11: 193–205. https://doi.org/10.21037/tcr-21-1601.

[39] Puliga E, Corso S, Pietrantonio F, Giordano S. Microsatellite instability in Gastric Cancer: Between lights and shadows. Cancer Treatment Reviews. 2021; 95: 102175. https://doi.org/10.1016/j.ctrv.2021.102175.

[40] Jiang P, Gu S, Pan D, Fu J, Sahu A, Hu X, *et al*. Signatures of T cell dysfunction and exclusion predict cancer immunotherapy response. Nature Medicine. 2018; 24: 1550–1558. https://doi.org/10.1038/s41591-018-0136-1.

[41] Patel TH, Cecchini M. Targeted Therapies in Advanced Gastric Cancer. Current Treatment Options in Oncology. 2020; 21: 70. https://doi.org/10.1007/s11864-020-00774-4.

[42] Chen C, Wang Z, Xi B, Xu Z, Zhao C, Hu W, *et al*. Focusing on DC cells to optimize the prediction of prognosis and innovative treatment strategies for colon cancer. Scientific Reports. 2025; 15: 17298. https://doi.org/10.1038/s41598-025-01792-8.

[43] Ma H, Qiu Q, Tan D, Chen Q, Liu Y, Chen B, *et al*. The Cancer-Associated Fibroblasts-Related Gene COMP Is a Novel Predictor for Prognosis and Immunotherapy Efficacy and Is Correlated with M2 Macrophage Infiltration in Colon Cancer. Biomolecules. 2022; 13: 62. https://doi.org/10.3390/biom13010062.